

Gravitational Waves from Stellar Collapse: Correlations to Explosion Asymmetries

Chris L. Fryer

Theoretical Astrophysics, Los Alamos National Laboratories,
Los Alamos, NM 87544

Daniel E. Holz

Center for Cosmological Physics
University of Chicago
Chicago, IL 60637

Scott A. Hughes

Department of Physics
Massachusetts Institute of Technology
Cambridge, MA 02139-4307

ABSTRACT

The collapse of massive stars not only produces observable outbursts across the entire electromagnetic spectrum but, for Galactic (or near-Galactic) supernovae, detectable signals for ground-based neutrino and gravitational wave detectors. Gravitational waves and neutrinos provide the only means to study the actual engine behind the optical outbursts: the collapsed stellar core. While the neutrinos are most sensitive to details of the equation of state, gravitational waves provide a means to study the mass asymmetries in this central core. We present gravitational wave signals from a series of 3-dimensional core-collapse simulations with asymmetries derived from initial perturbations caused by pre-collapse convection, core rotation, and low-mode convection in the explosion engine itself. A Galactic supernovae will allow us to differentiate these different sources of asymmetry. Combining this signal with other observations of the supernova, from neutrinos to gamma-rays to the compact remnant, dramatically increases the predictive power of the gravitational wave signal. We conclude with a discussion of the gravitational wave signal arising from collapsars, the leading engine for long-duration gamma-ray bursts.

Subject headings: black hole physics—stars: black holes—stars: supernovae—stars: neutron

1. Introduction

The mechanism behind core-collapse supernovae (SNe) remains one of the longest outstanding problems in astrophysics. Whether or not simulations of stellar collapse produce explosions depends sensitively on the numerical implementations of the neutrino transport and the equation of state physics (Herant et al. 1994; Burrows, Hayes, Fryxell 1995; Janka & Müller 1996; Mezzacappa et al. 1998; Fryer & Warren 2002; Buras et al. 2003). 10% differences in this physics can make the difference between the success or failure of an explosion. But it may be that the sensitivity of the current simulations occurs only because theorists are missing essential aspects of physics in the core. For example, rotation in the core (Fryer & Heger 1998; Akiyama et al. 2003; Kotake, Yamada, & Sato 2003a; Fryer & Warren 2004), asymmetric collapse (Burrows & Hayes 1996; Fryer 2004a), one-sided convection due to oscillations (Blondin, Mezzacappa & DeMarino 2003), or the merger of modes (Scheck et al. 2003) may help or hinder the explosion.

The reason we know so little about the core and the resultant supernova explosion is because we have very few ways of directly observing the engine behind these explosions. The collapsed core is enshrouded by the outer layers of the star and it is not until the supernova shock reaches the edge of the star and becomes optically thin to photons that we can finally see the supernova. Then begins the laborious task of working back from the optical display to study the workings of the inner core. Although these observations (see Akiyama et al. 2003 and references therein), and observations of the neutron star remnant (see Lai, Chernoff, & Cordes 2001; Briskin et al. 2003 for reviews), have shown that the supernova explosion is almost certainly asymmetric, the level of asymmetry in the engine is very difficult to determine from these indirect methods. Gravitational waves and neutrinos provide the only means to directly probe the supernova engine.

Neutrinos have only been detected in SN 1987A (Hirata et al. 1987; Bionta et al. 1987), and gravitational waves (GWs) have yet to be conclusively detected in supernovae. Unfortunately, the signals of both are sufficiently weak to limit their detection to Galactic or near-Galactic supernovae (Neutrinos: Burrows, Klein & Gandhi 1998; GWs: Fryer, Holz & Hughes: FHH 2002; Dimmelmeier, Font & Müller 2002; Kotake, Yamada & Sato 2003b; Fryer & Warren 2004; Müller et al. 2004). Although predictions for the GW signal from stellar collapse have been much higher in the past (see FHH 2002; New 2003 for reviews), these predictions were based on stellar cores rotating much faster than even the fastest rotating supernova progenitors produced today (Heger, Langer & Woosley 2000). Modern progenitors of stellar collapse are only marginally, if at all, unstable to bar instabilities, and strong bar modes (the source of strong gravitational wave signals) do not occur in collapse calculations using these progenitors (Fryer & Warren 2004). Even if bars did form,

they form at low densities, and at most produce a marginally detectable signal at 10 Mpc (Rampp, Müller & Ruffert 1998; FHH 2002). GW observations, like neutrinos, are limited to Galactic or near-Galactic supernovae.

Even though the rate of such nearby SNe are low (0.02 year^{-1}), the insight gained from these supernovae will provide essential information into stellar collapse. In this paper, we will focus on 3 phases of gravitational waves:

- I) **Stellar Bounce** - The signal produced during the bounce caused when the stellar core reaches nuclear densities and its runaway free-fall is abruptly halted. For initial progenitors with asymmetries or rotation, the quadrupole moment in the progenitors will vary wildly during bounce, producing a strong signal.
- II) **Convection** - The signal produced during the convective phase of the supernova engine. Even if the initial conditions are symmetric, the convection modes may merge to form low-mode convection with a significant time-variable quadrupole moment.
- III) **Neutrinos** - The signal produced by asymmetries in the neutrino emission. Asymmetries in the collapse or in the convection will lead to asymmetries in the neutrino emission. These asymmetries lead to a time-variable quadrupole moment.

The GW signal can not only be used to distinguish these phases, but also the asymmetry that causes the signal in each phase.

In this paper, we will use the results from recent 3-dimensional collapse simulations (Fryer & Warren 2002, 2004; Fryer 2004a) to study the different characteristics of these signals, focusing especially on what these signals can tell us about stellar collapse and supernova explosions. But a lot of uncertainty remains in such simulations and we use comparisons with other work and analytic estimates to gauge the uncertainties in these calculations. The models, and the numerical methods used to calculate the GW signal, are discussed in §2. §3 shows the results of these simulations, along with comparisons to other work and analytic estimates. To make GWs a powerful probe of the inner core, we must study a bigger picture and correlate the GW signal with other supernova observables: neutrino signal, nucleosynthetic yields and other explosion asymmetry characteristics in the observations (§4). We conclude with a discussion of the observability of gamma-ray bursts under the collapsar model and a review of the key observations and the constraints they can place on the supernova engine.

2. Computations

The gravitational wave signals presented here are derived from the 3-dimensional core-collapse calculations by Fryer & Warren (2002,2004) and Fryer (2004a). This core-collapse code couples smooth particle hydrodynamics (SPH) with a 3-flavor ($\nu_e, \bar{\nu}_e, \nu_{\mu,\tau}$) flux-limited diffusion neutrino transport scheme (Warren, Rockefeller, & Fryer 2004). Beyond a trapping radius (corresponding to an optical depth, $\tau_\nu = 0.03$), the neutrinos are assumed to escape the star completely. The neutrinos leaking from the “boundary particles” at this radius dominate the observed neutrino flux. Unless otherwise specified, the gravity is Newtonian, using the tree-based algorithm described in Warren & Salmon (1995). These models begin with initial stars that are both rotating and non-rotating, with density distributions that are either initially symmetric, or perturbed by global asymmetries (Table 1).

The advantage of such a code is that we can model the collapse of the entire star in 3-dimensions for a series of initial conditions with existing computational resources (a typical simulation takes roughly 100,000 processor hours on both the Space Simulator and ASCI Q machines). Because the full 3-dimensional star is modeled, no approximations need be taken to calculate the mass quadrupole moments and its derivatives. And since this code is Lagrangian (particle based), the resolution follows the proto-neutron star and this code is ideally suited to model asymmetries that accelerate this central core.

However, bear in mind that the neutrinos are modeled with a single-energy flux-limited transport algorithm. Comparison of such a transport algorithm with more sophisticated transport algorithms in 1 and 2-dimensions have found that the such calculations can drastically change the fate of the collapsing star (Buras et al. 2003). Note also that these models assume Newtonian rather than General Relativistic gravity, which not only affects the bounce of and convective motions in the core, but also forces us to calculate the gravitational wave signal using a post-process technique. All of our results must be tempered by these uncertainties.

However, as we shall see in §3, the gravitational wave signal is so weak that the back-reaction of the gravitational wave emission is unlikely to effect the dynamics in the core. The remaining uncertainties are less easy to quantify, but by comparing to more detailed 2-dimensional work (Müller et al. 2004), we can estimate the level of uncertainty in our results (§3).

We calculate the gravitational wave signal from baryonic mass motions using the

formulism of Centrella & McMillan (1993):

$$\begin{aligned} c^8/G^2 \langle (rh_+)^2 \rangle &= \frac{4}{15}(\ddot{I}_{xx} - \ddot{I}_{zz})^2 + \frac{4}{15}(\ddot{I}_{yy} - \ddot{I}_{zz})^2 + \frac{1}{10}(\ddot{I}_{xx} - \ddot{I}_{yy})^2 \\ &+ \frac{14}{15}(\ddot{I}_{xy})^2 + \frac{4}{15}(\ddot{I}_{xz})^2 + \frac{4}{15}(\ddot{I}_{yz})^2, \end{aligned} \quad (1)$$

$$c^8/G^2 \langle (rh_\times)^2 \rangle = \frac{1}{6}(\ddot{I}_{xx} - \ddot{I}_{yy})^2 + \frac{2}{3}(\ddot{I}_{xy})^2 + \frac{4}{3}(\ddot{I}_{xz})^2 + \frac{4}{3}(\ddot{I}_{yz})^2, \quad (2)$$

where r is the distance to the source. The angle brackets in these equations denote averaging over all source orientations, so that for example

$$\langle (rh_+)^2 \rangle = \frac{1}{4\pi} \int d\Omega r^2 h_+(\theta, \phi)^2. \quad (3)$$

The quantities \ddot{I}_{ij} are the second time derivatives of the trace-free quadrupole moment of the source. The diagonal elements are given by, for example,

$$\ddot{I}_{xx} = \frac{2}{3} \sum_{p=1}^N m_p (2x_p \ddot{x}_p - y_p \ddot{y}_p - z_p \ddot{z}_p + 2\dot{x}_p^2 - \dot{y}_p^2 - \dot{z}_p^2), \quad (4)$$

where m_p is the mass of an SPH particle, and (x_p, y_p, z_p) is its coordinate location. The other diagonal elements can be obtained using Eq. (4) plus cyclic permutation of the coordinate labels: $\ddot{I}_{xx} \rightarrow \ddot{I}_{yy}$ via $x \rightarrow y, y \rightarrow z, z \rightarrow x$; $\ddot{I}_{xx} \rightarrow \ddot{I}_{zz}$ via $x \rightarrow z, y \rightarrow x, z \rightarrow y$. The off-diagonal elements are given by, for example

$$\ddot{I}_{xy} = \sum_{p=1}^N m_p (x_p \ddot{x}_p + y_p \ddot{y}_p + 2\dot{x}_p \dot{y}_p), \quad (5)$$

the remaining off-diagonal elements can be found via symmetry ($\ddot{I}_{ji} = \ddot{I}_{ij}$) plus cyclic permutation. This approach provides only averaged square amplitudes, instead of the specific amplitude of the gravitational wave signal. This paper is concerned with general qualitative features of the wave signals, rather than detailed predictions. In this vein, the averaged square amplitudes are a cleaner and more effective description.

For the trends we are studying here, this formulism is sufficient and provides a cleaner signal.

For gravitational waves from neutrinos, we use the formulae derived by Müller & Janka (1997):

$$\begin{aligned} (h_{xx}^{\text{TT}})_{\text{pole}} &= \frac{2G}{c^4 r} \int_{-\infty}^{t-R/c} dt' \\ &\int_{4\pi} d\Omega' (1 + \cos\theta') \cos(2\phi') \frac{dL_\nu(\Omega', t')}{d\Omega'}, \end{aligned} \quad (6)$$

$$(h_{xx}^{\text{TT}})_{\text{equator}} = \frac{2G}{c^4 r} \int_{-\infty}^{t-R/c} dt' \int_{4\pi} d\Omega' (1 + \sin\theta' \cos\phi') \frac{\cos^2\theta' - \sin^2\theta' \sin^2\phi'}{\cos^2\theta' + \sin^2\theta' \sin^2\phi'} \frac{dL_\nu(\Omega', t')}{d\Omega'}. \quad (7)$$

where G is the gravitational constant, c is the speed of light and r is the distance of the object. $(h_{xx}^{\text{TT}})_{\text{pole}}$ denotes the emergent strain for an observer situated along the source coordinate frame's z-axis (or pole) and $(h_{xx}^{\text{TT}})_{\text{equator}}$ is the comparable strain for an observer situated perpendicular to this z-axis (or equator). For our simulations, the rotation axis or asymmetry axis is the z-axis and the polar view corresponds to the axis of symmetry for the initial perturbations.

In SPH calculations, these expressions reduce to:

$$(h_{xx}^{\text{TT}})_{\text{pole}} = \frac{2G}{c^4 R} \sum \Delta t \sum_{p=1}^N (1 \pm z/r) (2x^2/r^2 - 1) \Delta L_\nu, \quad (8)$$

$$(h_{xx}^{\text{TT}})_{\text{equator}} = \frac{2G}{c^4 R} \sum \Delta t \sum_{p=1}^N (1 \pm \sqrt{1 - z^2/r^2}(x, y)/r) \frac{z^2/r^2 - \sqrt{1 - z^2/r^2}(x, y)^2/r^2}{z^2/r^2 + \sqrt{1 - z^2/r^2}(x, y)^2/r^2} \Delta L_\nu. \quad (9)$$

where Δt is the timestep, the summation is over all particles emitting neutrinos that escape this star (primarily, the boundary particles). We assume that the neutrino emission at these boundaries is along the radial direction of the particle, so ΔL_ν is set to $E_\nu/\Delta t$ where E_ν is the neutrino energy emitted by that particle. If the neutrinos are more isotropic, this will weaken the gravitational wave signal, but not by more than a factor of 2. The \pm correspond to observers along the positive/negative directions of each axis: for instance, in the polar equation, this corresponds to the positive/negative z-axis. In the equatorial region, the x,y axis is determined by the choice of x or y position for the (x,y) coordinate in the equation.

3. Results from 3-dimensional Simulations

A massive star ends its life when its iron core becomes so massive that the thermal and electron degeneracy pressure of the star can no longer support the core and it implodes. This implosion continues until the core reaches nuclear densities, where nuclear forces and neutron degeneracy pressure halt the collapse. The “bounce” of the core does not produce an explosion. The bounce shock stalls when neutrino cooling and photodisintegration saps the shock of its energy. If there are asymmetries in the star, this collapse and bounce phase produces rapidly varying quadrupole moments and gravitational waves.

The stalled shock leaves behind a convectively unstable region between the proto-neutron star and the accretion shock of the infalling star. Neutrinos leaking out of the proto-neutron star heat this region, driving further convection. When the pressure from this convection overcomes the pressure of the infalling star, a supernova explosion is launched. The mass motions in this convection also produce rapidly varying quadrupole moments.

If stellar asymmetries or convective motions are sufficiently asymmetric, the neutrino emission will also be asymmetric. These neutrino asymmetries can produce a significant gravitational wave signal. As we shall see, these signals can dominate the GW signal in some cases.

Let’s take a closer look at each of these phases in turn, using core-collapse simulations as a guide.

3.1. Gravitational Waves from Core Bounce

Rotation: Although massive stars are observed to rotate at nearly break-up velocities while on the main-sequence, the angular velocity (of the envelope at least) decreases dramatically (just from angular momentum conservation) when these stars expand into giants. If their cores are not coupled to their expanding envelopes, they will spin up as the core contracts. If they are coupled, the contracting core will impart its angular momentum to the envelope and slow down as this envelope expands. The extent of this coupling depends sensitively on uncertain magnetohydrodynamic physics and current supernova models (Heger, Langer, & Woosley 2000; Heger, Woosley, & Spruit 2004) predict a range of answers (see Fryer & Warren 2004 for a review). If these cores collapse with significant angular velocity, centrifugal support will deform the collapse, making strong asymmetries and, ultimately, a strong gravitational wave signal. GW observations provide an ideal means to probe this asymmetry.

Figure 1 shows the gravitational wave signals for a range of rotating stellar collapses. Model Rot1 is the the fastest spinning core produced by Heger, Langer & Woosley (2000). The signal in Fig. 1 assumes the collapse occurs 10 kpc away. At 10 kpc (within the Galaxy), this bounce signal from models Rot1 and Rot2 (peaking at 2×10^{-21} at ~ 1 kHz) is well above the expected noise level of advanced LIGO, suggesting it should not be difficult to observe. The strong signal dies away very quickly and is strongest right at core bounce. But the strength of this signal depends sensitively on the rotation. The slower rotating cores do not produce gravitational wave signals (Rot3) that are significantly stronger than

those produced by asymmetries (Rot4 and Rot5)¹ in a non-rotating core.

Asymmetries from Explosive Burning: Rotation is not the only way to produce asymmetries in the star just prior to collapse. Explosive burning in the oxygen and silicon shells produces strong convection in these shells, causing density perturbations in these shells (Bazan & Arnett 1998). If this convection has many downflows and upflows (high mode convection), these density perturbations would be randomly distributed across the oxygen and silicon layers of the star, similar to the 5-10% perturbations introduced using the smooth particle hydrodynamics technique. The signal from our non-rotating star (Figs. 1,2) is caused by these perturbations.

But what if the convection is dominated by low modes with the density perturbations taking on a more global scale? Burrows & Hayes (1996) argued that global perturbations from oxygen and silicon burning would lead to asymmetries in the bounce and could be the source of neutron star kicks. Lai & Goldreich (2000) argued that this convection would drive oscillatory modes in the iron core that would grow during collapse and drive large asymmetries in the bounce. Fryer (2004a) mimicked these global perturbations by decreasing the density to the oxygen and silicon layers (or in the entire star) in a cone on the positive z axis.

Fig. 3 shows the gravitational wave signals from these globally asymmetric explosions. The bounce signal from these global asymmetries is much different than that of the rotating stars. The peak signal does not occur at bounce, but 10-20 ms later. The signal from baryonic mass motions is dominated by the asymmetries caused by the oscillations in the core as ejecta and neutrino asymmetries kick the neutron star.

Models Asym1, Asym2 correspond to the large asymmetry cases for “Shell Only”, or “With Oscillations” simulations in Fryer (2004a). Models Asym3, Asym4 are 30% perturbations in the oxygen/silicon burning shells. Asym3 and Asym4 differ in that the momentum imparted by the last scattering of neutrinos is included in Asym3 and not in Asym4². Note that there is very little difference between the GW signal of these two models. Neither model produces sizable kicks ($v_{\text{kick}} < 30\text{km s}^{-1}$) in the neutron star or strong oscillations in the core. Models Asym1 and Asym2 produce much stronger oscillations and slightly stronger GW signals. The largest signal occurs when oscillatory modes are driven

¹Our SPH initial conditions introduce $\sim 5\text{-}10\%$ asymmetries. Although these are numerical artifacts, they do not differ significantly from the asymmetries expected from explosive burning prior to collapse.

²The flux limited-diffusion scheme used by Fryer (2004a) includes the effects of neutrino pressure and momentum. Below $\tau_\nu = 0.03$, we make a light-bulb approximation. At the boundary, the neutrino momentum must be included. The prescription for this is described in Fryer (2004a).

in the iron core prior to collapse (Asym1). However, as we shall see in §3.3, the neutrino GW signal for these models is much stronger than that of mass motions, and that will dominate the signal at late times.

Fig. 4 compares the gravitational wave signals from the extreme cases of rotating (Rot1) and globally asymmetric (Asym1) simulations along with a non-rotating model (SPH1 - equivalent to high mode perturbations). For mass motions, the rotating model has the strongest signal which peaks at bounce. The globally asymmetric model can also produce a signal which should be detectable by LIGO, peaking at ~ 10 -20 ms after bounce. If the rotation or asymmetries are not extreme, the gravitational wave signal will not be easily detectable. However, even a non-detection will tell us much about the core, as it will rule out these large (or larger) asymmetries in the initial core.

3.2. Gravitational Waves from Convection

With accurate equations of state, when the bounce shock stalls, it leaves behind an unstable entropy profile above the proto-neutron star. The region bounded by the proto-neutron star on the inside and the accretion shock where the rest of the material falls down onto the stalled bounce shock quickly becomes convective. This convection is further driven by heating from neutrinos leaking out of the proto-neutron star. Convection allows the energy deposited from neutrinos to convert into kinetic energy of rising matter. When this matter is able to push off the infalling star, an explosion is launched (see Fryer 1999 for a review).

Herant et al. (1994) found that the energy in this convection was primarily carried in just a few upflows and Herant (1995) argued that if the convection were dominated by a single upflow, they could explain the high space velocities of pulsars (see §4.3). Indeed, the convective modes merge with time (Fig. 5). In our 3-dimensional models, the explosion occurs so quickly that there are still ~ 3 -6 upflows when the explosion is launched. Hence, the convective modes do not produce a strong signal for our models (Figs. 1-4). Indeed, the only simulations that produced strong signals from baryonic mass motions were the globally asymmetric collapse simulations with strongly oscillating neutron stars.

However, Scheck et al. (2003) have found that for sufficiently delayed explosions (which may well be more typical in supernovae), the convective upflows can merge until there is only 1 single upflow. This can produce a gravitational wave signal that rivals even the bounce signal for some rotating stars (Müller et al. 2004). To get a better understanding of this signal, we can approximate the mass motions by assuming that the convective motions

have merged, leading to a single downflow, but that the downflow occurs in spurts (large blobs accreting). Such an assumption is not too unreasonable, as mass builds up at the accretion shock until its weight carries it down, punching its way through the upflowing material. To estimate the maximum signal from convection, we assume the mass of the accreting blob is $0.1 M_{\odot}$ and it accelerates at free-fall from the edge of the accretion region to half way between the accretion shock and the proto-neutron star surface (at 50 km), at which point they begin to decelerate and stop at the proto-neutron star surface (we chose a deceleration that was symmetric in magnitude about the half radius). The signal produced by this “convection” varies as the blob falls. Figure 6 plots the maximum of that signal as a function of the accretion shock radius. As the convection region expands, the signal will decrease, but it could take 500 ms for the shock to move from 100 km to 500 km. Note that this signal is an upper limit to the possible signal from convection and is an order of magnitude higher than that predicted by Müller et al. (2004). It is also nearly an order of magnitude greater than the rotating simulations presented here.

3.3. Gravitational Waves from Neutrino Asymmetries

All of these asymmetries in the bounce and convection lead to asymmetries in the neutrino emission. These asymmetries produce a gravitational wave signal that grows with time. In most cases, the asymmetry in the neutrinos is not large enough to dominate the GW signal (e.g. Müller et al. 2004), but neutrino asymmetries can dominate the gravitational wave signal in the case of asymmetric collapse (e.g. Burrows & Hayes; Fryer 2004a).

Figs. 7 and 8 show the gravitational wave signal from models Asym1 and Asym2 respectively. The signal continues to grow with time and, for these two simulations, exceeds the bounce or convective signals by over an order of magnitude! Unfortunately, these signals were not calculated for any models prior to Fryer (2004a), so we can not present gravitational wave signals for earlier models. But the neutrino asymmetry in the rotating and spherical models are more than ~ 2 orders of magnitude less than the asymmetries of these simulations, so neutrinos asymmetries may not play a dominant role in most supernovae. Indeed, Müller et al. (2004) found that the GW signal from asymmetric neutrino emission was slightly lower than that produced by baryonic mass motions.

Figures 7 and 8 show the GW signal from neutrinos along 6 lines of site (positive and negative x, y, and z axes). The magnitude of the signal is strongest along the positive z axis (the positive z axis is where the initial density perturbation was placed). Reviewing all axes gives a handle on how observation location will effect the signal. These extreme

asymmetries will easily produce signals detectable in a Galactic supernova. In addition, the time evolution of this signal is significantly different that it can easily be distinguished from signals by mass motions. Unfortunately, unlike the signal from mass motions, the signal for neutrinos peaks at lower frequencies (Fig. 9) and, in advanced LIGO sensitivity band, the neutrino asymmetry GW signal is only slightly stronger than mass motions for these stellar implosions.

Detecting a Galactic supernova in gravitational waves and following the time evolution of the GW signal can easily tell us much about the behavior of the inner core of a star during collapse. We can distinguish between rotating and asymmetric collapse and between low-mode and high-mode convection. We can also estimate the level of neutrino asymmetry. Gravitational waves provide an ideal window into the mass motions in, and just above, the proto-neutron star core.

4. Comparing with other Observables

Especially with Galactic supernovae, we have a number of additional observations which can be used to help learn about supernovae ranging from direct observations of the core with neutrinos to indirect methods such as supernova asymmetries, nucleosynthetic yields, and studies of the compact remnant from these explosions. Combined with these constraints, gravitational waves can tell us much about the supernova engine.

4.1. Neutrinos

Neutrino detections provide the only other means beyond GWs to study the supernova engine directly. SuperKamiokande will detect over 5000 neutrinos from a supernova 10 kpc away (Burrows, Klein, & Gandhi 1998). The bulk of these detections will be electron anti-neutrinos, but both SuperKamiokande and the Sudbury Neutrino Observatory will detect a few hundred electron and μ neutrinos. This signal will be sufficient to produce reasonable neutrino light-curves that can be used to make detailed comparisons with the neutrino emission predicted by models.

How do the mass motions affect the neutrino observations? The actual net asymmetries in the neutrino emission tend to be small (a percent or less - see Janka & Mönchmeyer 1989a, 1989b), but Kotake et al. (2003a) have found that rotation can lead to a neutrino energy that varies by as much as a factor of 2 for different angular lines-of-sight. Figure 10 shows the electron neutrino luminosity and energy for a range of models (from spherical to

rotating to asymmetric collapse). For our models, the electron neutrino luminosity does not change much even though the actual progenitors for these objects does vary in some cases. The electron neutrino energies vary by $<30\%$. However, bear in mind that these calculations rely upon a single-energy flux-limited diffusion scheme and we should take these quantitative results with a grain of salt.

The μ , τ , and electron anti-neutrinos vary much more than the electron neutrinos (Figs. 11-12). Even so, it would be very difficult to distinguish asymmetries in the core with neutrinos. But neutrinos do give us an ideal probe into the equation of state in the core (e.g. Pons et al. 2000). The details of the equation of state will also affect the gravitational waves to a lesser extent (Dimmelmeier et al. 2002) and we can use neutrino observations to distinguish equation of state effects from mass motions. Combining the neutrino and the gravitational wave signal, we can study both the mass asymmetries in the collapse and the behavior of matter at nuclear densities. Quantitative analyses will require much more detailed core-collapse models.

The detection of both gravitational waves and neutrinos also has implications for calculating the neutrino mass. The delay between the emission of neutrinos (t_e) and their arrival at a detector (t_d) is (e.g. Arnett & Rosner 1987):

$$t_d - t_e \approx (d/c)(1 + 0.5m_\nu^2/E_\nu^2) \quad (10)$$

where d is the distance from the supernova to the observer, c is the speed of light and m_ν, E_ν are the mass and energy of the neutrino respectively. If we know that our GW signal peaks at bounce (as is the case for our rotating supernovae), the time between the peak emission of the gravitational and neutrino signals should not differ by more than 5 ms and can easily be determined to this accuracy. By differencing the delay in the neutrinos by the delay in the gravitational wave signal $(t_d - t_e)_\nu - (t_d - t_e)_{\text{GW}}$, we could then determine the neutrino mass from a 10 kpc supernova to better than 1 eV (see also, Arnaud et al. 2002). It will be more difficult to use this technique if the neutrino signal is determined by convective modes or neutrino asymmetries, where the timing is less accurate.

4.2. Observations of Explosion Asymmetries

The same asymmetric mass motions that produce gravitational waves may also produce asymmetries in the supernova explosion. For example, rotation causes the strongest convection to occur along the rotation axis and this bipolar convection will drive asymmetric explosions (Fryer & Heger 2000; Kotake et al. 2003a; Fryer & Warren 2004). The merger of convective modes will also produce wildly asymmetric supernovae (Scheck et al. 2003).

Burrows & Hayes (1996) also argued that asymmetric collapse would produce asymmetries in the explosion, but 3-dimensional calculations have found that these asymmetries are mild (Fryer 2004a).

For Galactic supernovae, there are many observational diagnostics that can help, albeit indirectly, determine the level of asymmetry in the core. Supernova 1987A provides a number of examples of how powerful these diagnostics can be for nearby supernovae and modern telescopes. One of the surprises SN 1987A provided for astronomers was that somehow the nickel in the core was mixed well into the star, causing the gamma-ray luminosity powered by the ^{56}Ni produced in this explosion to peak 150 d earlier than expected by theorists (Pinto & Woosley 1988). Spherical explosions can not explain this easily (Kifonidis et al. 2003), but mild (~ 2 times stronger along the rotation axis over the equator) asymmetries would easily explain this mixing (Fig. 13: Hungerford, Fryer, & Warren 2003, Fryer 2004b). Because of these asymmetries, the nickel is also ejected preferentially along the asymmetry axis (Fig. 14) and this asymmetric distribution leads to a gamma-ray line profile that, in principal, can determine the angle and level of the asymmetry (with some uncertainty due to the degeneracy of these two effects: Hungerford et al. 2003). Supernova 1987A was too distant to easily make these distinctions, but a Galactic supernova with modern telescopes would provide strong constraints.

Asymmetries also effect the nucleosynthetic yields, optical line profiles, and polarization of supernovae. Varying the shock velocity changes the yields from explosive nuclear burning. Nagataki et al. (1998) found that mild asymmetries (on the same level as those required to explain the gamma-ray lines) were required to best fit the nucleosynthetic yields of SN 1987A. Interpretations of the polarization signal have argued that most supernovae must be jet-like with explosions 100 times stronger along the rotation axis over the equatorial plane (Akiyama et al. 2003). However, this interpretation requires several layers of detailed radiation transport calculations. This result is in contrast to more direct measurements from both radio studies of supernovae (Berger et al. 2003) and specific studies of SN 1987A (e.g. the mixing and nucleosynthetic yield results described above) which argue for mild asymmetries. It is likely that the interpretation of the polarization measurement is overestimating the asymmetry and such large asymmetries are probably limited to a small fraction of all supernovae. But this discrepancy highlights the limitations of such indirect measurements of asymmetries.

What indirect observations from current supernovae can tell us at this point is that asymmetries exist. The situation will change with a Galactic supernova. A Galactic supernova will provide enough gamma-ray photons (which have few transport uncertainties) to constrain not only the level of asymmetry, but the axis of asymmetry. Such information

can be used to help us understand the GW signal and use gravitational waves to constrain the mass motions.

4.3. Compact Remnants

Asymmetric mass motions also affect the velocity and spin of the neutron star remnant produced in the supernova explosion. Spinning, magnetized neutron stars are observed as pulsars. For the fastest spinning collapse progenitors (the ones that produce sizable GW signals), the angular momentum is so high in the core that, if no angular momentum were lost in the supernova explosion, the resultant core would be spinning at sub-millisecond periods. During the collapse and subsequent supernova explosion of the core, the high angular momentum in the core is ejected, but the newly-born neutron star will have periods in the 1-3 ms range, with total rotational energies in excess of 10^{51} ergs (Fryer & Warren 2004). If such a pulsar had moderate to high (above 10^{11} G) magnetic fields, its emission would easily be observable in the Galaxy (even if not directed toward us!). Indeed, the pulsar emission may alter the supernova explosion energy (see Fryer & Warren 2004). A detailed, strong GW signal (or the lack of a signal) could give constraints on this emission. Similarly, pulsar observations can help interpret the GW signal. Since the pulsar spin depends primarily on the rotation of the core, it is most sensitive to this source of gravitational waves. A number of limitations may confuse such results: e.g. the neutron star could lose angular momentum due to GW driven modes after the explosion, some collapsing stars produce fast-spinning neutron stars but only weak GW signals.

The evidence that neutron stars receive a sizable “kick” ($\sim 500 \text{ km s}^{-1}$) at birth continues to grow (see Lai, Chernoff, & Cordes (2001); Briskin et al. (2003) for recent reviews). These kicks are either produced by ejecta asymmetries (e.g. Herant 1995; Burrows & Hayes 1996; Scheck et al. 2003) or neutrino asymmetries (Lai & Arras 1999; Fryer 2004a). It is likely that the velocity of the neutron star remnant of a Galactic supernova will be measured. The velocity of the neutron star does not depend so much on the rotation, but may depend on the level of asymmetry in the collapse (Burrows & Hayes 1996; Fryer 2004a) or the merger of convective modes (Herant 1995; Scheck et al. 2003). Because these two GW mechanisms have such distinct signatures, GW observations of a Galactic supernova (combined with a neutron star velocity measurement) will be able to determine which, if either, of these mechanisms produce neutron star kicks.

5. Conclusions

A number of asymmetries in the stellar collapse can produce a gravitational wave signal in a Galactic supernova that should be detectable by advanced LIGO. These asymmetries are caused by rotation in the star, asymmetries induced by explosive nuclear burning just prior to collapse, or low mode convection in the supernova engine. Each has a distinctive gravitational wave signal which can be used to study the mass motions in the supernova engine.

But the real power of GWs arises when combined and corroborated with other observations. The correlation between GW and these observations is summarized in Tables 2 and 3. Fast rotating progenitors can produce a strong signal at bounce, mild asymmetries in the ejecta and fast-spinning neutron star remnants. The timing of the GW signal is within 5 ms (maybe even closer) of the neutrino signal and such an event could be used to constrain the neutrino mass. Asymmetries in the collapsing star caused by explosive burning can produce strong signals at late times through asymmetric neutrino emission and mild velocities on the neutron star, but the explosion is roughly symmetric. Low mode convection will produce a gravitational wave signal during the convective engine phase, asymmetric explosions and possibly strong neutron star kicks. The GW signal will help determine the mechanism behind the SN and our understanding of these additional phenomena.

Supernovae are not the only explosions produced by stellar collapse. The favored mechanism for long-duration gamma-ray bursts, the collapsar model (Woosley 1993; MacFadyen & Woosley 1999), invokes the collapse of a massive star. Collapsars are massive stars that do not produce strong supernova explosions, but instead collapse to form black holes. If the star is rotating fast enough, the high angular momentum stellar material will form an accretion disk around the black hole. Energy liberated from the disk drives a strong explosion (even stronger than supernovae) in a jet along the rotation axis.

Because rotation is required to produce a collapsar explosion, the collapsing stars will necessarily be fast rotators. Thus they will have a strong bounce GW signal. However, this signal is unlikely to be much stronger than our fast rotating collapse models (too much rotation will also prevent the collapsar engine from working - MacFadyen & Woosley 1999). It is likely that collapsars arise from extremely massive stars (Heger et al. 2003), but, because the cores of massive stars are essentially all the same, this does not alter the GW signal significantly from our extreme rotating case (Dupuis, Fryer, & Heger 2004).

The bounce of collapsar driven gamma-ray bursts will only be detectable when they occur in the galaxy. The accretion onto the black hole will cause ringing, but this signal

too will only be detectable in a Galactic gamma-ray burst. Finally, for the low-mass disks produced in collapsars (Popham, Fryer, & Woosley 1998; MacFadyen & Woosley 1999), no disk instabilities will form and the accretion phase of collapsars are unlikely to produce strong GW signals. The narrowly collimated, low-baryon jet produced in collapsars will produce a signal akin to neutrino driven signals. However, for a bipolar jet, there will be no signal along the jet axis. Perpendicular to the jet axis, the signal (using equation 8) can be as high as 5×10^{-24} for a 10^{51} erg jet, on par with the signal from the disk, but still only detectable within the Galaxy and only if the jet is not directed toward us (so not associated with GRBs, but maybe with hypernovae). What this all boils down to is that collapsar driven gamma-ray bursts, like supernovae, will not be detectable beyond the Galaxy. Given their low rate ($\sim 10^{-5}\text{year}^{-1}$ in the Galaxy), collapsars will not be a strong GW source. However, other gamma-ray burst models will produce strong GW signals (e.g. neutron star mergers) and GWs can easily distinguish these two burst engines.

It is a pleasure to thank L. S. Finn whose questions set up the direction of this paper. This work under the auspices of the University of Arizona and the U.S. Dept. of Energy, and supported by its contract W-7405-ENG-36 to Los Alamos National Laboratory as well as DOE SciDAC grant number DE-FC02-01ER41176, NSF grant PHY-0244424 and NSF Grant PHY-0114422 to the CfCP. The simulations used in this work were run on LANL's ASCI Q machine and the Space Simulator.

Table 1. Collapse Models

Model Name	Reference Name	Initial Rot. (rad s ⁻¹)	Initial Asymmetry	Number of Particles
Rot1	SN15A-hr ^a	4	symmetric	5×10^6
Rot2	SN15B ^a	10	symmetric	5×10^5
Rot3	SN15C ^a	0.25	symmetric	10^6
Rot4	SN15B-nr ^a	0	symmetric	10^6
Rot5	SN15A-nr ^a	0	symmetric	10^6
Sph1	Model C ^b	0	symmetric	3×10^6
Sph2	Model B ^b	0	symmetric	10^6
Sph3	Model A ^b	0	symmetric	3×10^5
Asym1	Shell Only ^c	0	40% in O,Si ^d	10^6
Asym2	With Oscillations ^c	0	25% in Fe,O,Si ^d	10^6
Asym3	Shell Only ^e	0	30% in O,Si ^d	10^6
Asym4	Shell Only ^e	0	30% in O,Si ^{d,f}	10^6

^aFryer & Warren (2004)

^bFryer & Warren (2002)

^cFryer (2004a)

^dThis refers to the density decrease in a 30° cone along the positive z axis either in just the O, Si layers (Shell Only) or the entire star (With Oscillations).

^eSimulations first presented here, but using the same conditions as in Fryer (2004a).

^fBackreaction from momentum carried away by neutrinos not included.

Table 2. Collapse Results

Model Name	Peak GW Signal (10^{-21} at 10 kpc)	f(Hz) at Peak ^a	Pulsar Period	NS Velocity km s^{-1}	Asymmetry $v_{\text{pole}}/v_{\text{eq}}$
Rot1	2.3	~ 1000	$> 0.66 \text{ ms}$	< 30	~ 2
Rot2	1.9	~ 1000	$> 0.35 \text{ ms}$	< 30	~ 1.5
Rot3	0.5	~ 1000	$> 17 \text{ ms}$	< 30	< 1.1
Rot4	0.4	~ 100	$> 1 \text{ s}$	< 30	< 1.1
Rot5	0.5	~ 200	$> 1 \text{ s}$	< 30	< 1.1
Sph1	0.1	~ 200	$> 1 \text{ s}$	< 30	< 1.1
Sph2	0.1	~ 100	$> 1 \text{ s}$	< 30	< 1.1
Sph3	0.1	~ 100	$> 1 \text{ s}$	< 30	< 1.1
Asym1	0.9	$\sim 1000^{\text{b}}$	$> 1 \text{ s}$	~ 200	~ 1.2
Asym2	0.4	$\sim 1000^{\text{b}}$	$> 1 \text{ s}$	< 100	~ 1.2
Asym3	0.2	$\sim 1000^{\text{b}}$	$> 1 \text{ s}$	< 30	< 1.1
Asym4	0.3	$\sim 1000^{\text{b}}$	$> 1 \text{ s}$	< 30	< 1.1

^aBecause most of the signals are dominated by a single burst, this frequency is just t_{burst}^{-1} where t_{burst} is the burst duration.

^bThis is the frequency of the baryonic mass motions. Neutrino asymmetries dominate the signal below this frequency, peaking below 10 Hz.

Table 3. GW sources in Core-Collapse

Initial Asymmetry	Source	Gravitational Waves		Correlation		
		Peak GW Signal ^a	$T_\nu - T_{\text{GW}}$	Expl. Asym.	ms Pulsar	NS Kick
None	Convection ^b	10^{-22}	50-500ms	Y?	N	Y?
Rotation	Bounce ^b	2.5×10^{-22}	0 ms	Y	Y	N
Density ^c	Neutrinos	$> 4 \times 10^{-22}$	50ms-1s	N	N	Y?

^aat 10 kpc

^bBaryonic mass motions drive signal.

^cDensity Perturbation caused by explosive shell burning prior to collapse.

REFERENCES

- Akiyama, S., Wheeler, J. C., Meier, D. L., & Lichtenstadt, I. 2003, *ApJ*, 584, 954
- Arnett, D. & Rosner, J. L. 1987, *PRL*, 58, 1906
- Arnaud, N., Barsuglia, M., Bizouard, M. A., Cavalier, F., Davier, M., Hello, P., Pradier, T. 2002, *PRD*, 65, 3010
- Bazan, G., & Arnett, D. 1998, *ApJ*, 496, 316
- Berger, E., Kulkarni, S. R., Frail, D. A., Soderberg, A. M., submitted to *ApJ*
- Bionta, R. M., Blewitt, G., Bratton, C. B., Caspere, D., Ciocio, A. 1987, *PRL*, 58, 1494
- Blondin, J. M., Mezzacappa, A., DeMarino, C. 2003, *ApJ*, 584, 971
- Briskin, W. F., Fruchter, A. S., Goss, W. M., Hernstein, R. S., & Thorsett, S. E. 2003, accepted by *ApJ*
- Buras, R., Rampp, M., Janka, H.-Th., Kifonidis, K. 2003, *PRL*, 90, 241101
- Burrows, A., Klein, D., Gandhi, R. 1992, *PRD*, 45, 3361
- Burrows, A., Hayes, J., & Fryxell, B. A. 1995, *ApJ*, 450, 830
- Burrows, A. & Hayes, J. 1996, *Phys. Rev. Lett.* 76, 352
- Centrella, J. M., & McMillan, S. L. W. 1993, *ApJ*, 416, 719
- Dimmelmeier, H., Font, J. A., Müller, E. 2002, *A&A*, 393, 523
- Dupuis, R., Fryer, C. L., & Heger, A. 2004, in preparation
- Fryer, C. L. 1999, *ApJ*, 522, 413
- Fryer, C.L. & Heger, A., 2000, *ApJ*, 541, 1033
- Fryer, C. L., Holz, D. E., Hughes, S. A. 2002, 565, 430: FHH
- Fryer, C. L., & Warren, M. S. 2002, *ApJ*, 574, L65
- Fryer, C. L., & Warren, M. S. 2004, *ApJ*, 601, 391
- Fryer, C. L. 2004a, *ApJ*, 601, L175
- Fryer, C. L. 2004b, *NewAR*, 48, 13

- Gustafson, E., Shoemaker, D., Strain, K., Weiss, R. 1999, LSC White Paper on Detector Research and Development, LIGO Document T990080-00-D
- Heger, A., Langer, N., Woosley, S. E. 2000, ApJ, 528, 368
- Heger, A., Fryer, C. L., Woosley, S. E., Langer, N., Hartmann, D. 2003, ApJ, 591, 288
- Heger, A., Woosley, S. E., Spruit, H. 2004, in preparation
- Herant, M., Benz, W., Hix, W.R., Fryer, C.L. & Colgate, S.A. 1994, ApJ, 435, 339
- Herant, M. 1995, Space Science Reviews, 74, 335
- Hirata, K., Kajita, T., Koshiba, M., Nakahata, M., Oyama, Y. 1987, PRL, 58, 1490
- Hungerford, A. L., Fryer, C. L., Warren, M. S. 2003, ApJ, 594, 390
- Janka, H.-Th., & Mönchmeyer, R. (1998a), A&A, 209, L5.
- Janka, H.-Th., & Mönchmeyer, R. (1998b), A&A, 226, 69
- Janka, H.-Th., & Müller, E. 1996, A&A, 306, 167
- Kotake, K., Yamada, S., Sato, K. 2003a, ApJ, 595, 304
- Kotake, K., Yamada, S., Sato, K. 2003b, PRD, 68, 4023
- Kifonidis, K., Plewa, T., Janka, H.-Th., Müller, E. 2003, A&A, 408, 621
- Lai, D. & Arras, P. 1999, ApJ, 519, 745
- Lai, D., Chernoff, D. F., & Cordes, J. M. 2001, ApJ, 549, 1111
- Lai, D. & Goldreich, P. 2000, ApJ 535, 402
- MacFadyen, A. I., Woosley, S. E. 1999, ApJ, 524, 262
- Mezzacappa, A., Calder, A. C., Bruenn, S. W., Blondin, J. M., Guidry, M. W., Strayer, M. R., Umar, A. S. 1998, Apj, 493, 848
- Müller, E., & Janka, H.-Th. 1997, A&A, 317, 140
- Müller, E., Rampp, M., Buras, R., Janka, H.-Th. 2003, accepted by ApJ
- Nagataki, S., Hashimoto, M., Sato, K., Yamada, S., Mochizuki, Y. 1998, ApJ, 492, L45
- New, K. C. B. 2003, Living Reviews in Relativity, IN-2003-2

- Pinto, P. A. & Woosley, S. E. 1988, *Nature*, 333, 534
- Pons, J., Reddy, S., Ellis, P. J., Prakash, M., Lattimer, J. M. 2000, *PRC*, 62, 5803
- Popham, R., Woosley, S. E., Fryer, C. L. 1999, *ApJ*, 518, 356
- Rampp, M., Müller, E., & Ruffert, M. 1998, *ApJ*, 332, 969
- Scheck, L., Plewa, T., Janka, H.-T., Kifonidis, K., & Müller, E. 2003, submitted to *Phys. Rev. Letters*.
- Warren, M.S., & Salmon, J.K. 1995, *Computer Physics Communications*, 87, 266
- Warren, M. S., Rockefeller, G., & Fryer, C. L. 2003, in preparation
- Woosley, S. E. 1993, *ApJ*, 405, 273

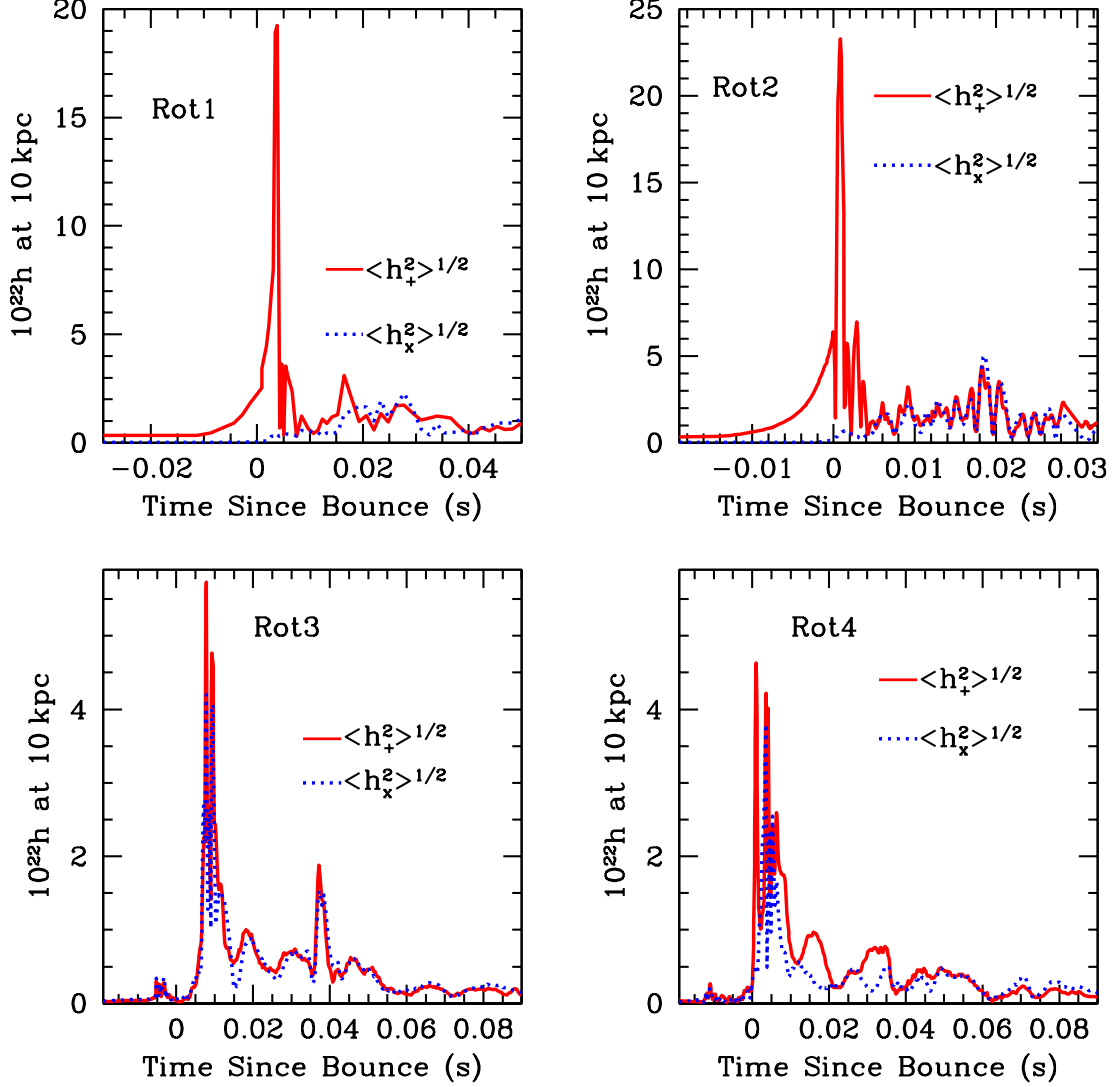


Fig. 1.— The angle averaged wave amplitudes ($\langle h_+^2 \rangle^{1/2}$: solid line, $\langle h_x^2 \rangle^{1/2}$: dotted line) for the mass motions from 4 rotating supernova models. Rot2 is the fastest rotating model. Rot3 is what would be predicted for a magnetically braked core. Rot4 shows the signal from the same star as Rot2, but where the rotation was set to zero just before collapse. See Table 1 for more details. Note that the gravitational wave signal is a factor of 5 higher in the rapidly versus slowly rotating models. A fast-rotating supernova in the Galaxy should be detectable by advanced LIGO.

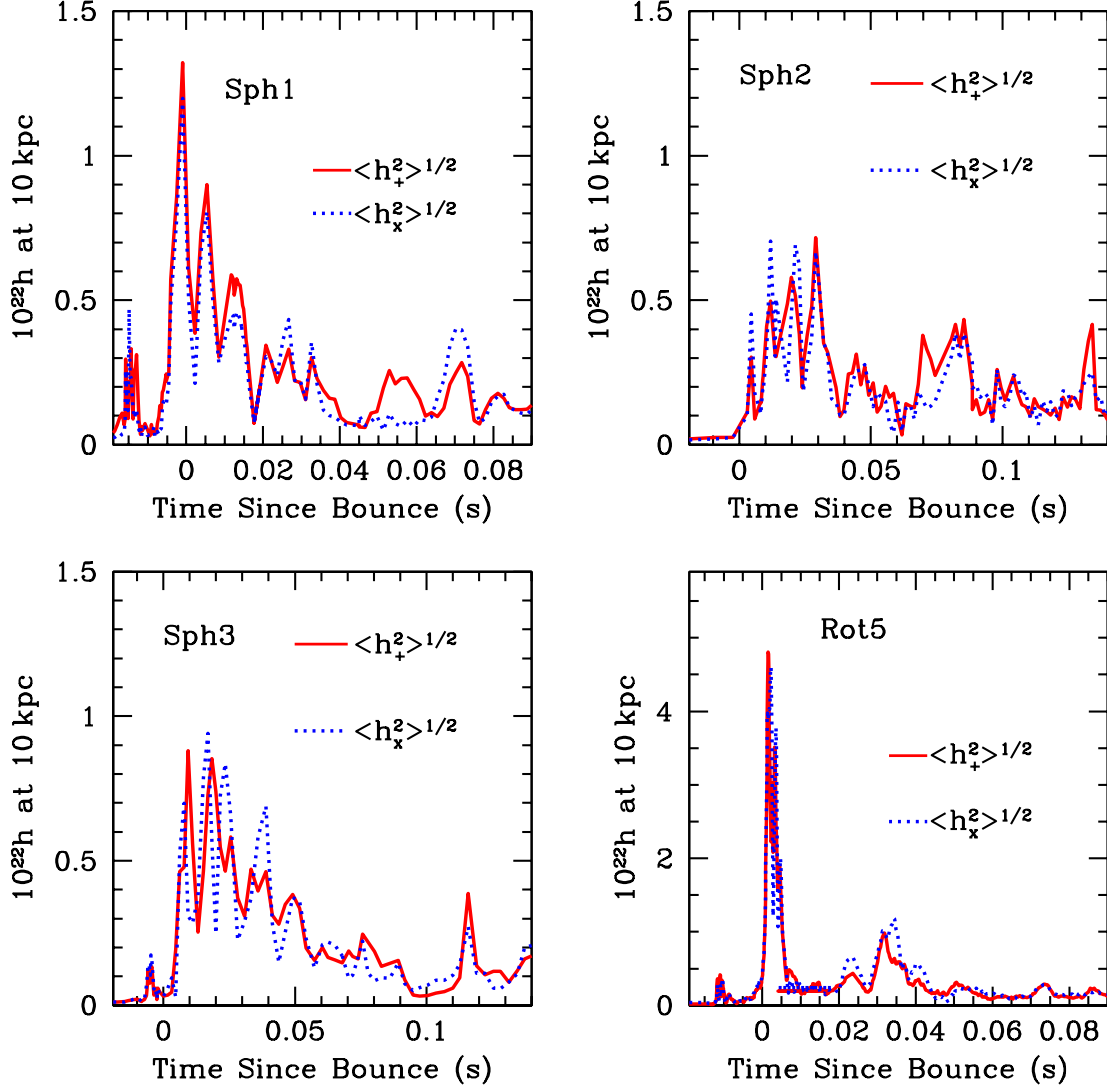


Fig. 2.— The angle averaged wave amplitudes ($\langle h_+^2 \rangle^{1/2}$: solid line, $\langle h_x^2 \rangle^{1/2}$: dotted line) for the mass motions from 4 non-rotating supernova models. Sph1-Sph3 are 3 different models with 3 levels of resolution (0.3, 1.0, 3.0 million particles). In these simulations, gravity was assumed to be spherically symmetric. Rot5 is a rotating progenitor (corresponding to Rot1: see Fig. 1) where the velocity angular was set to zero just before collapse, but with the collapse followed under full gravity. The difference in signals arises both from full versus spherically symmetric gravity and from the different progenitors.

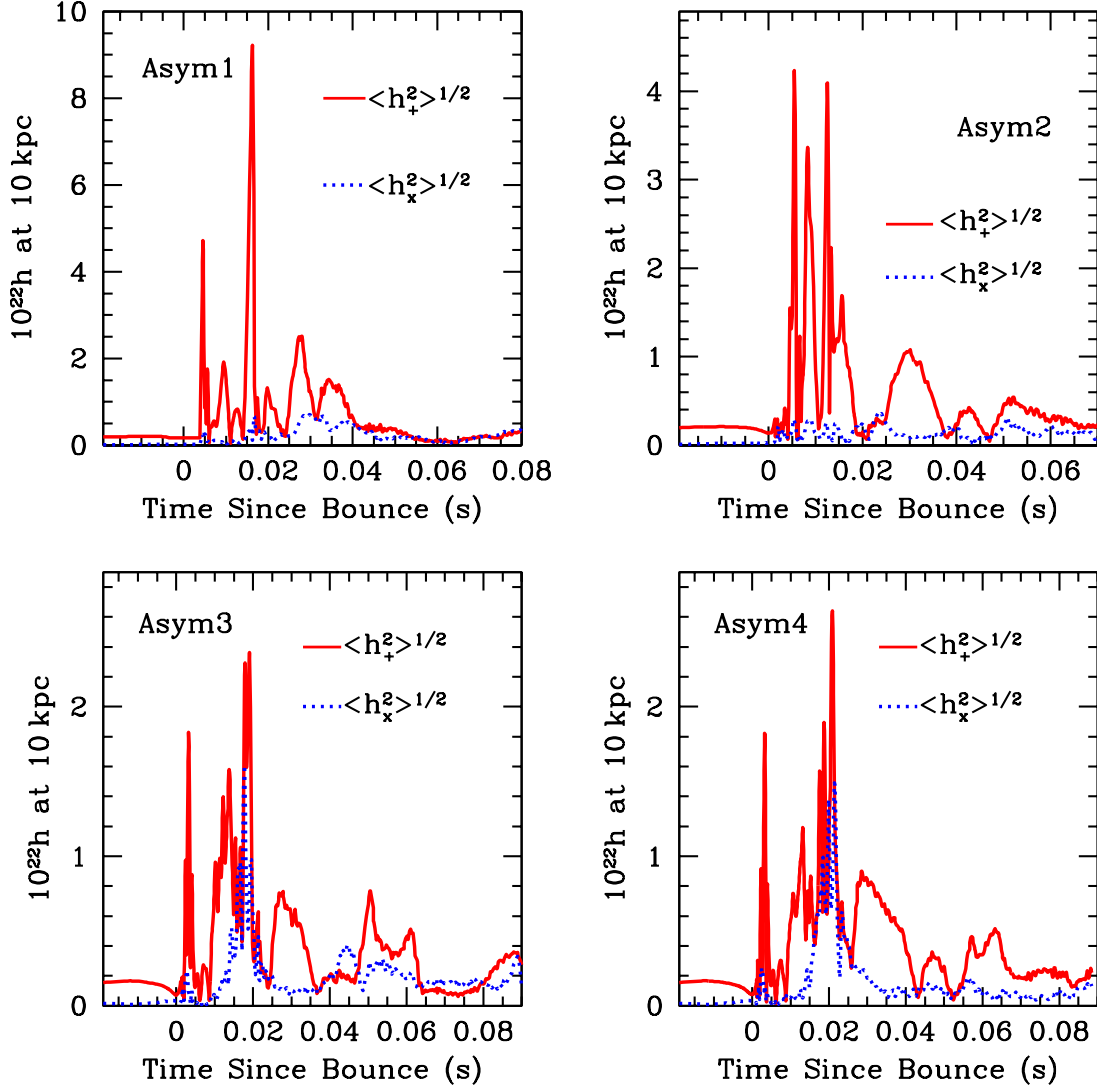


Fig. 3.— The angle averaged wave amplitudes ($\langle h_+^2 \rangle^{1/2}$: solid line, $\langle h_x^2 \rangle^{1/2}$: dotted line) for the mass motions from 4 supernovae with global perturbations prior to collapse. Asym1 corresponds to a 25% global perturbation throughout the entire core (assuming oscillatory modes in the neutron star). Asym2 corresponds to a 40% global perturbation in the burning shells only. Asym3 and Asym4 correspond to 30% perturbations in the burning shells, with and without momentum being carried away by neutrinos.

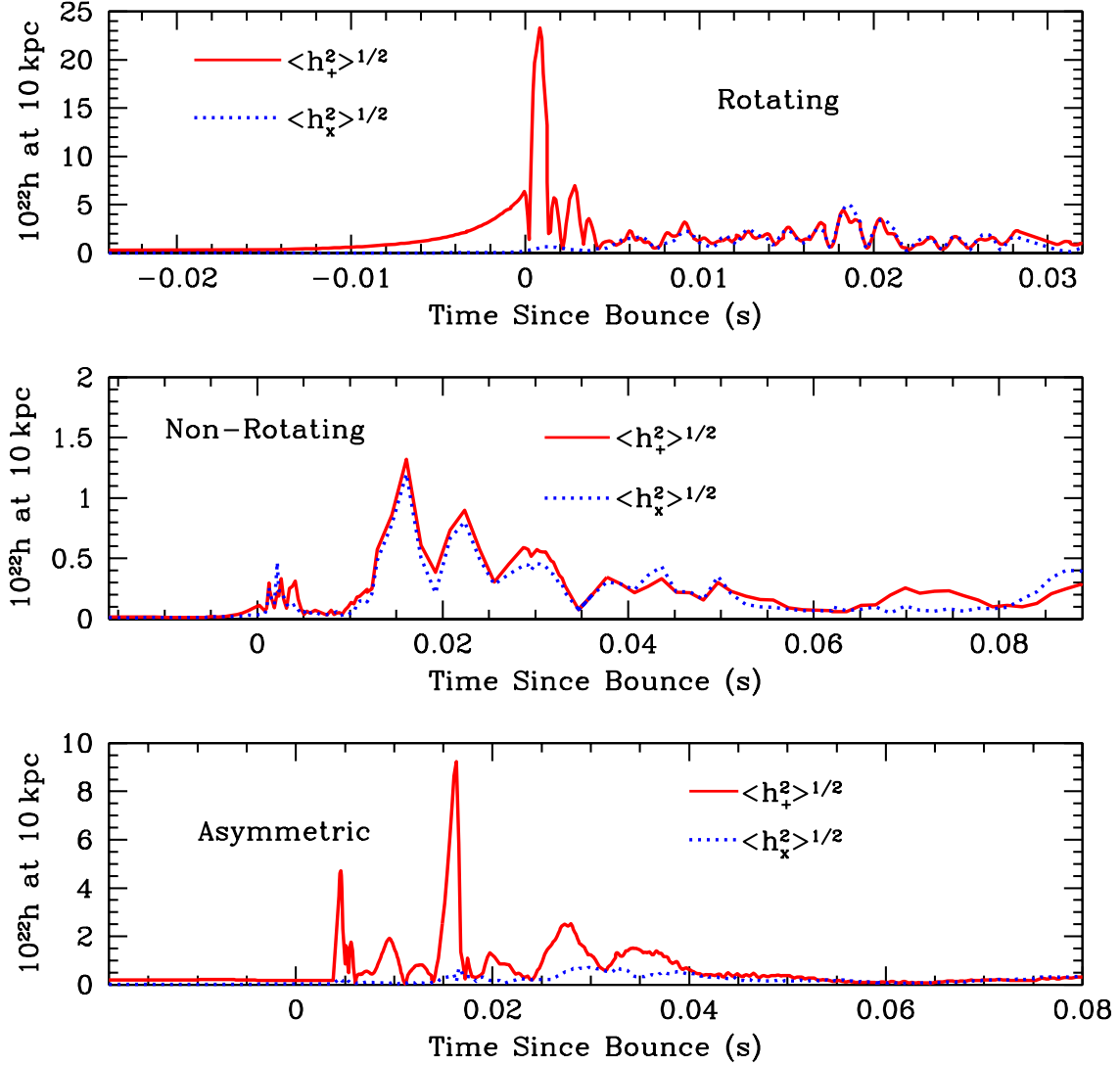
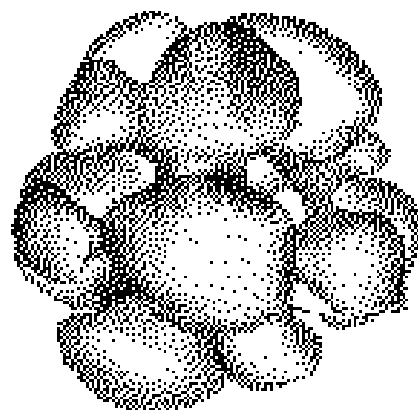


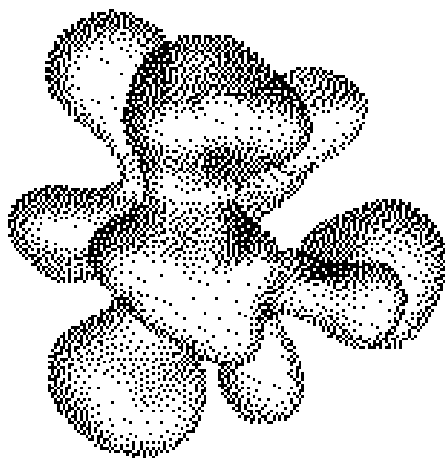
Fig. 4.— The angle averaged wave amplitudes ($\langle h_+^2 \rangle^{1/2}$: solid line, $\langle h_x^2 \rangle^{1/2}$: dotted line) for the mass motions from 3 representative models of rotating, non-rotating, and asymmetric collapse. The fast-rotator produces the strongest signal which occurs at bounce. The asymmetric collapse simulation produces a reasonably strong signal, but not necessarily at bounce, and the weak signal from the non-rotating case also does not peak at bounce.

200km



T=30ms

200km



T=50ms

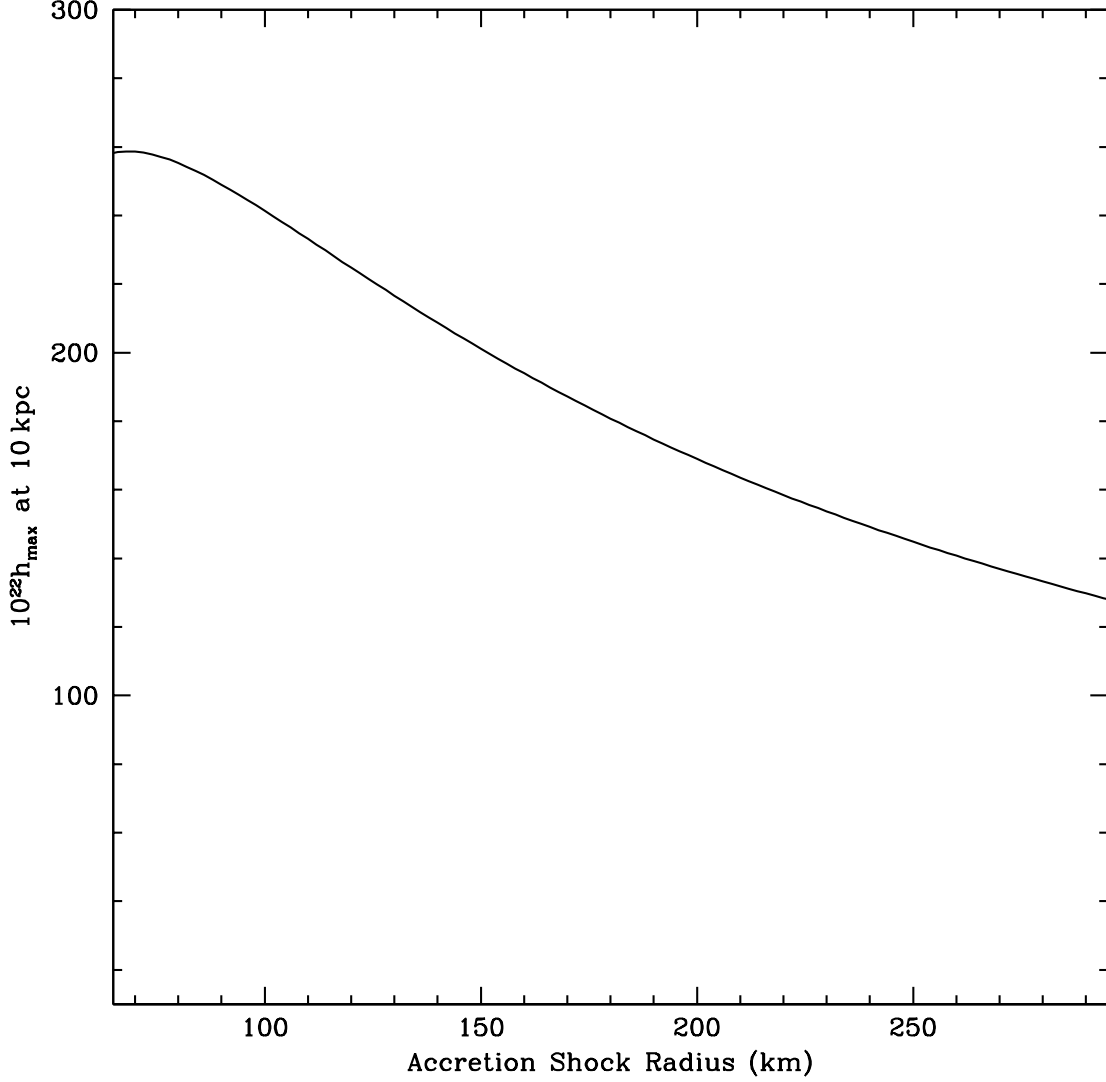


Fig. 6.— Maximum gravitational wave signal from convection as a function of the radial extent of the convective region. As the convective region expands, the maximum signal decreases. Note that this estimate is an upper limit, and calculations predict signals that are 1–2 orders of magnitude weaker than this value.

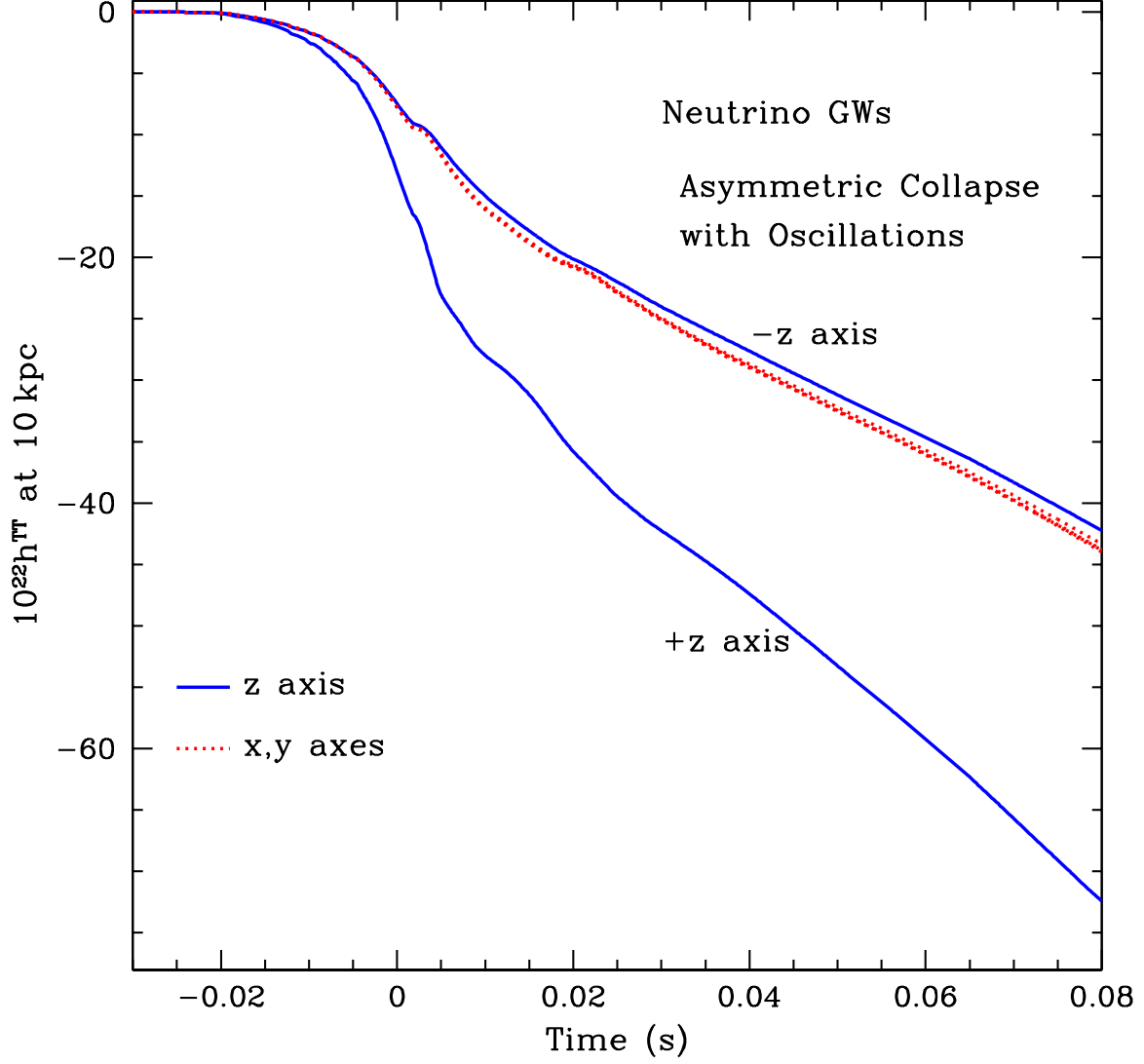


Fig. 7.— Gravitational wave signal for the simulation with a 25% core oscillation perturbation as a function of time and observer location. The signals observed off the perturbation axis are nearly all identical and are bracketed by the positive and negative z axis observations.

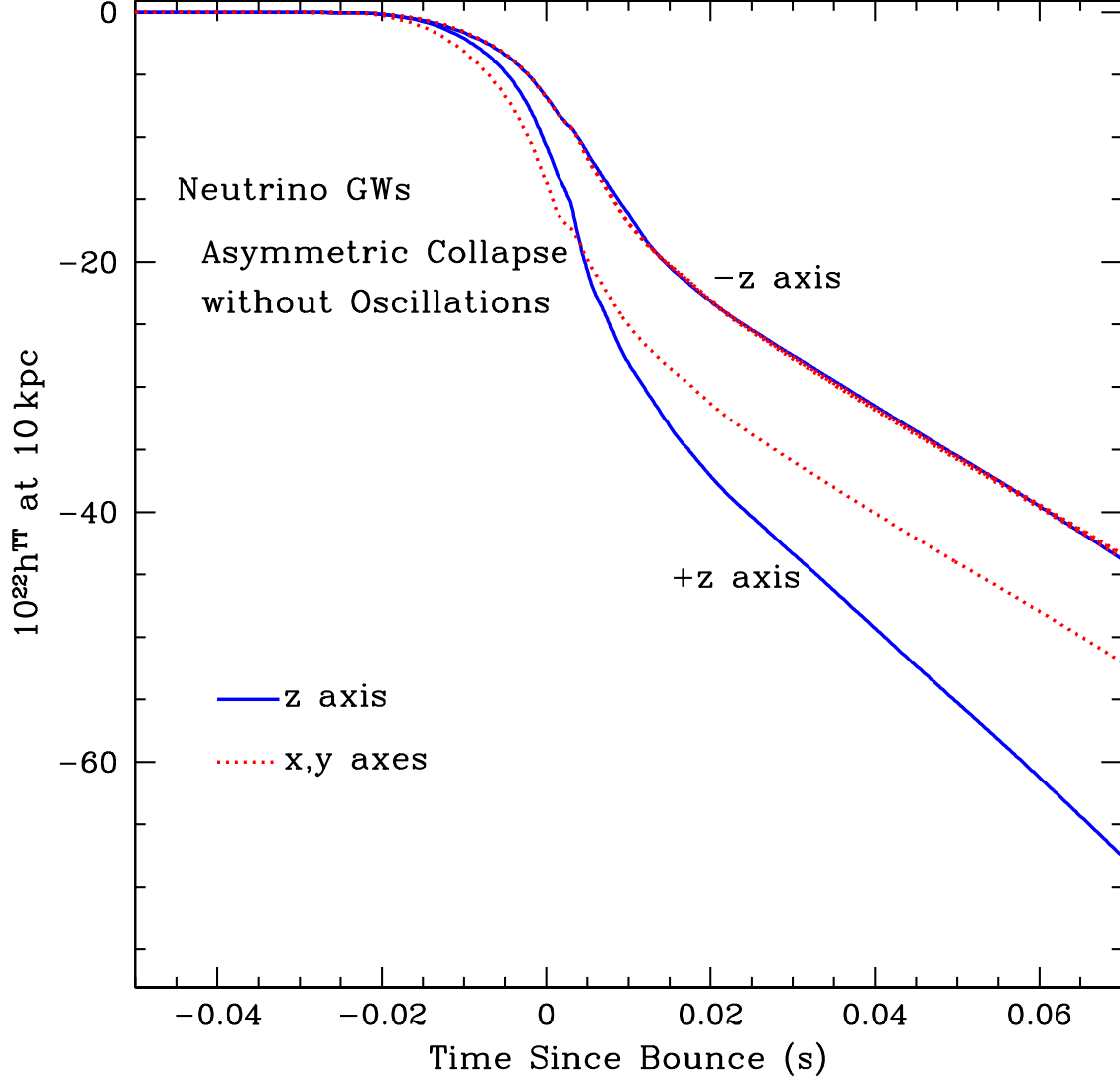


Fig. 8.— Gravitational wave signal for the simulation with a 40% burning shell perturbation as a function of time and observer location. As with Fig. 7, the signals observed off the perturbation axis are nearly bracketed by the positive and negative z axis observations.

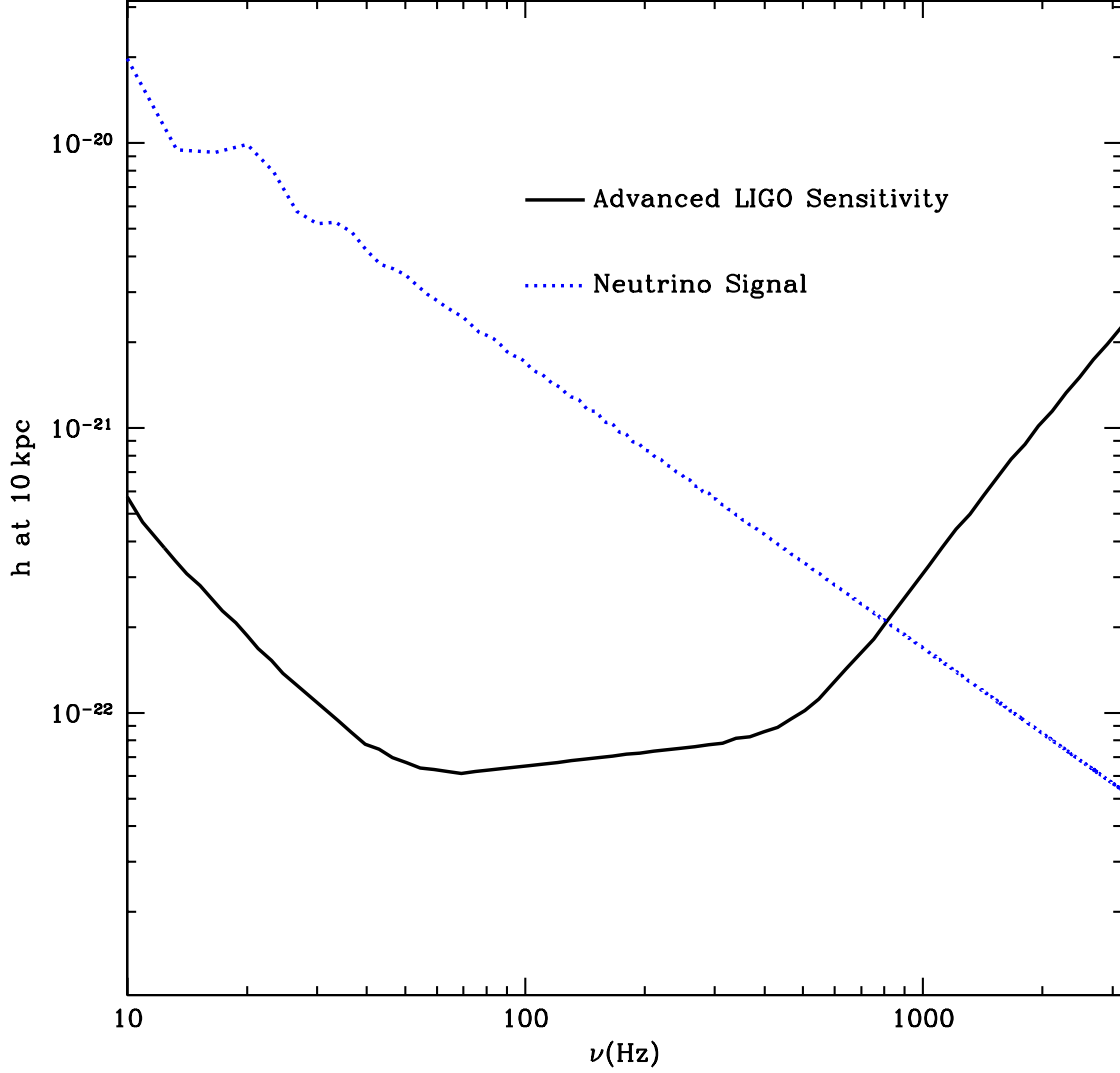


Fig. 9.— Spectral energy distribution (calculated by taking the Fourier transform of the data from fig. 7) of the GW radiation from the neutrino asymmetries for model Asym1 (25% perturbations throughout the star). The advanced LIGO noise curve is plotted for comparison (Gustafson et al. 1999). The neutrino signal for more reasonable asymmetries is likely to be an order of magnitude lower.

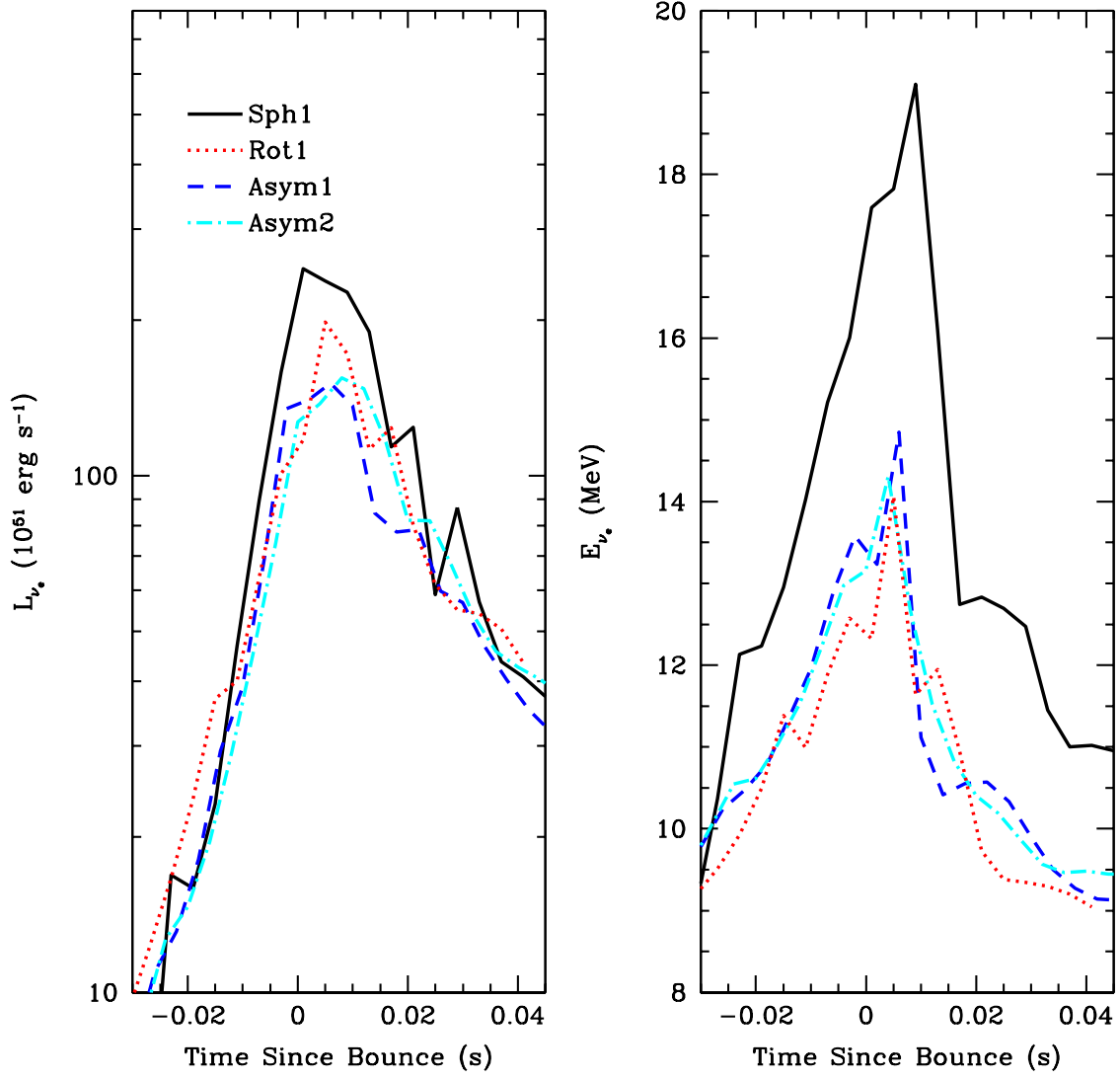


Fig. 10.— Electron neutrino luminosity and energy as a function of time since bounce. The luminosities (and energies to the 30% level) are all very similar. Based upon these simulations, it would be difficult to distinguish the mass motions from observations of just the the electron neutrinos.

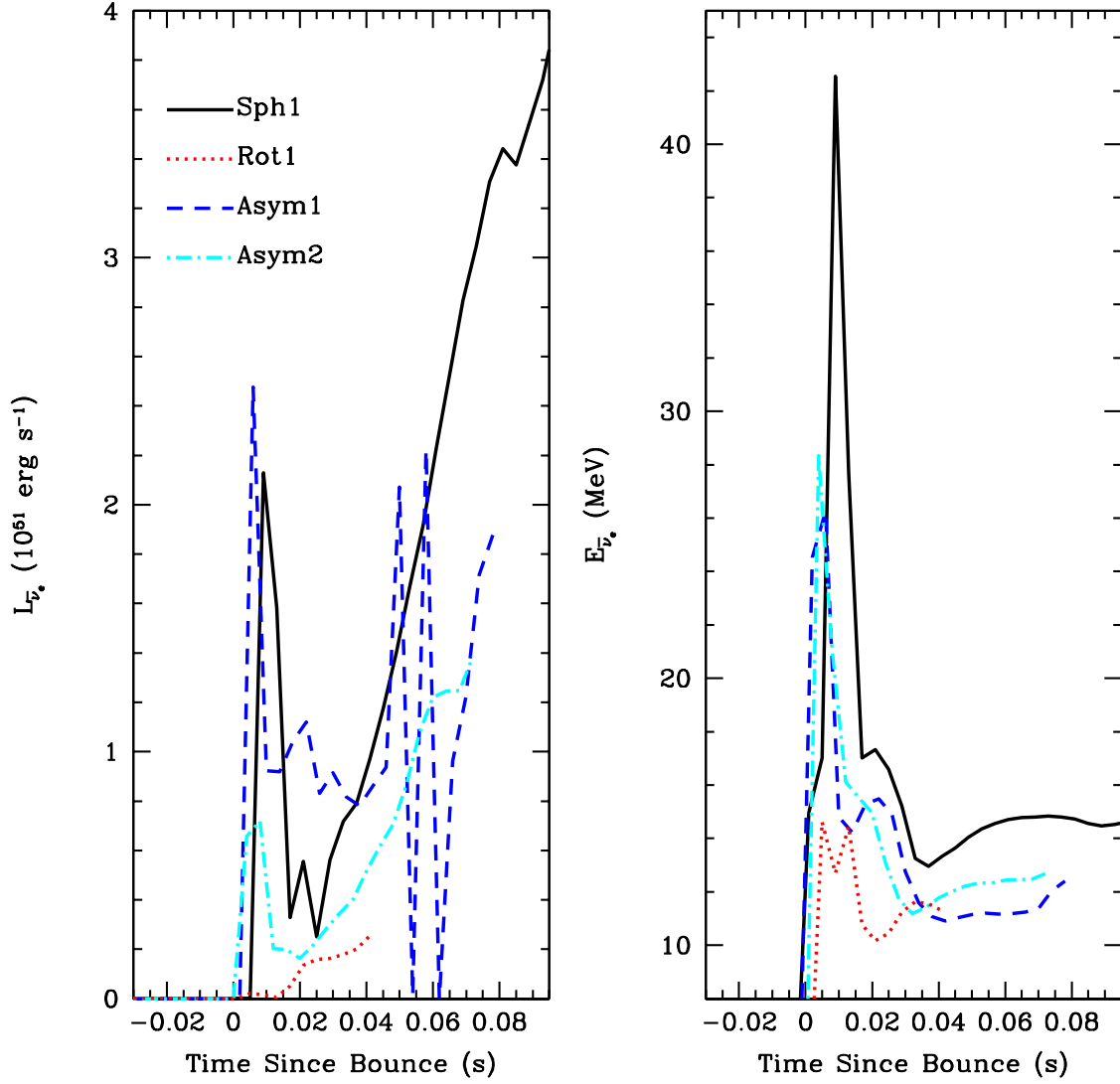


Fig. 11.— Anti-electron neutrino luminosity and energy as a function of time since bounce. The differences in the luminosities and energies are greater for these neutrinos than those of the electron neutrinos (Fig. 10), but the uncertainties (due to the lower fluxes) are higher for these models. Neutrino observations may be able to constrain the mass motions with more detailed 3-dimensional neutrino estimates.

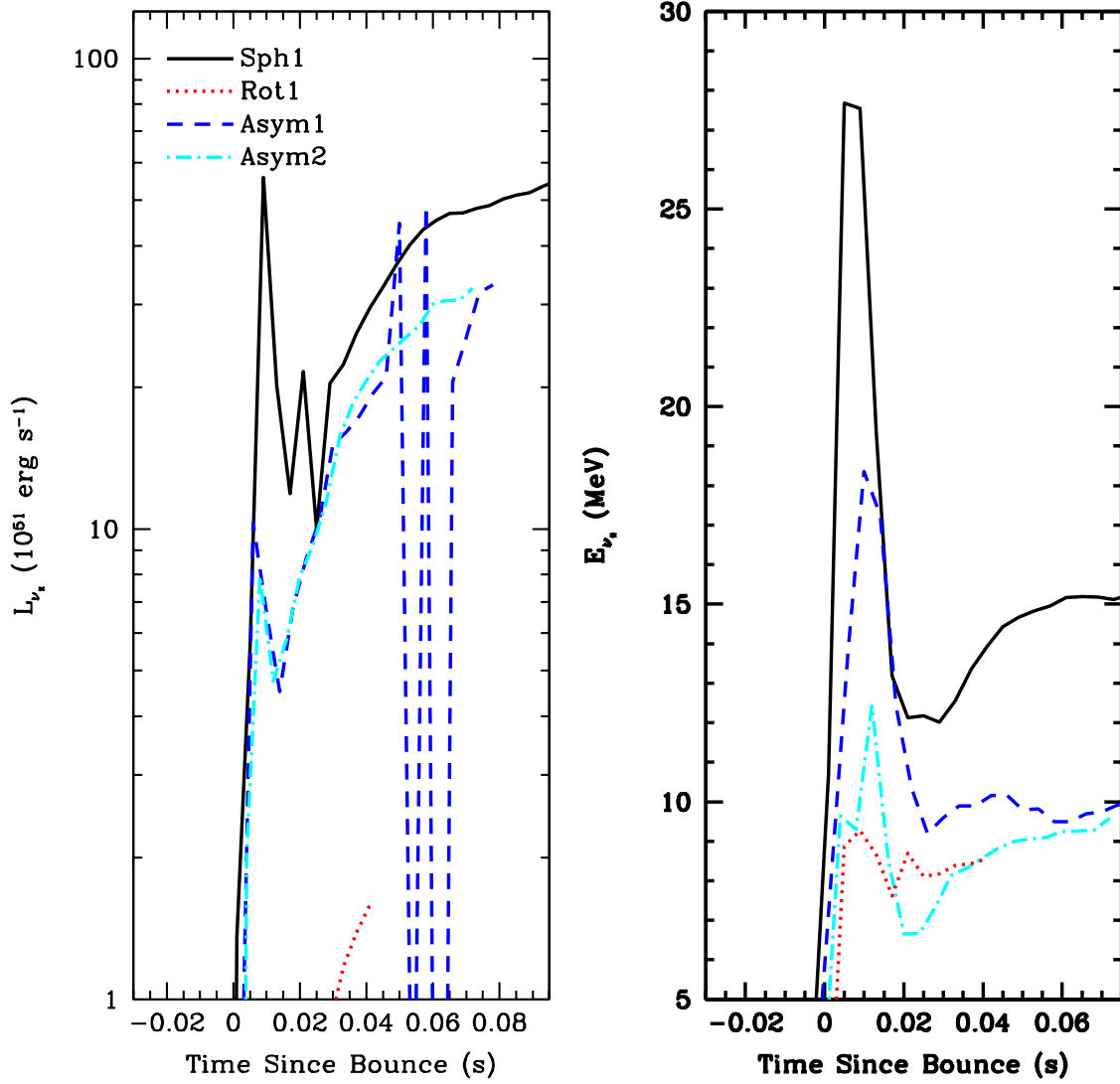


Fig. 12.— μ, τ neutrino luminosity and energy as a function of time since bounce. As with the anti-electron neutrinos, the differences in the luminosities and energies are greater for these neutrinos than those of the electron neutrinos (Fig. 10), but the uncertainties (due to the lower fluxes) are higher for these models. Anti-electron neutrino observations are easier to observe, and their observations will probably place stronger constraints on the mass motions and equation of state. etailed 3-dimensional neutrino estimates.

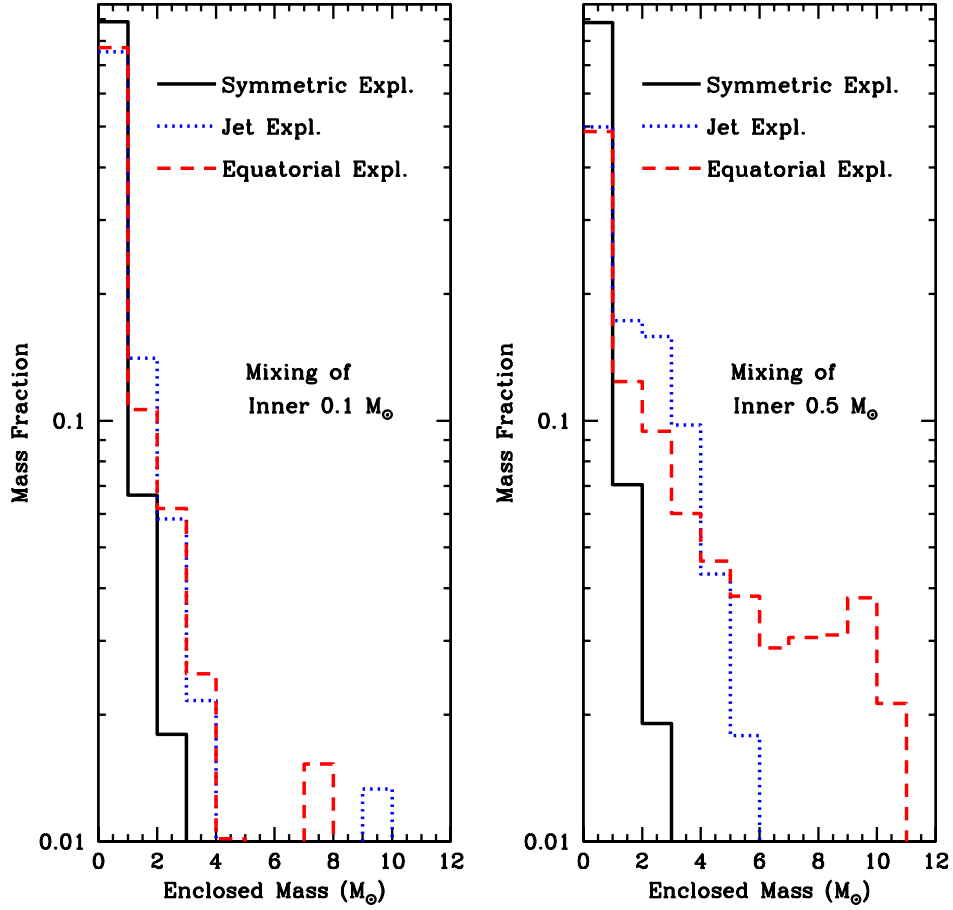


Fig. 13.— Amount of mixing of the inner $0.1 M_{\odot}$ (left) and the inner $0.5 M_{\odot}$ (right) of supernova ejecta for a symmetric explosion with decay energy added in (solid line), a polar explosion with a jet 2 times stronger along the poles than along the equator (dotted lines), and an equatorial explosion with the explosion 4 times stronger in the equator than along the poles (dashed line). See Hungerford et al. (2003) for details.

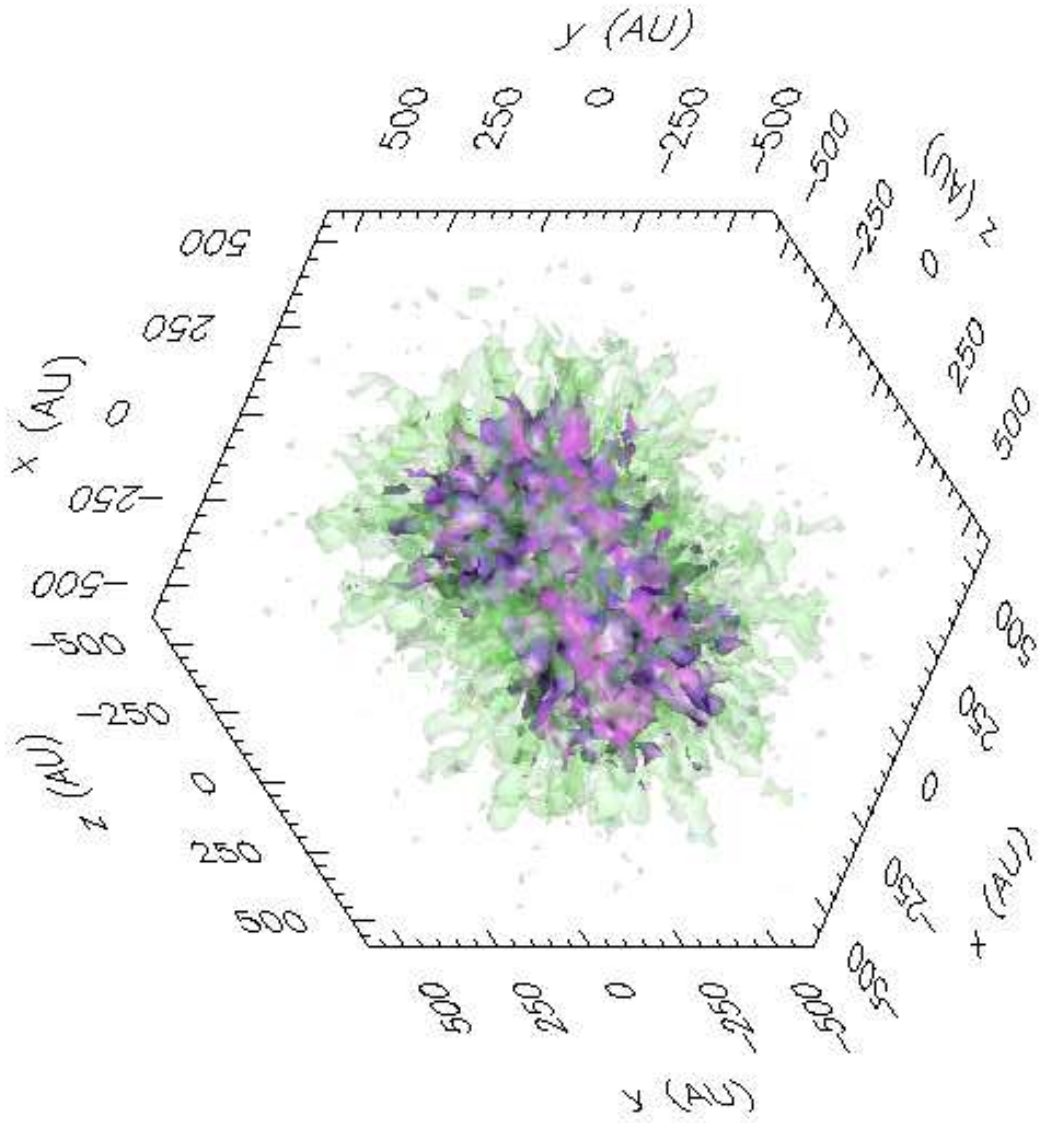


Fig. 14 — Two contours of the nickel distribution for an asymmetric explosion. The inner